Cavitation during Hot-Torsion Testing of Ti-6Al-4V

P.D. NICOLAOU, J.D. MILLER, and S.L. SEMIATIN

Hot-torsion testing was used to establish the cavitation behavior of a typical alpha/beta titanium alloy, Ti-6Al-4V, with a colony microstructure, during simple-shear deformation. For this purpose, sections of deformed specimens were examined by optical metallography, and by scanning and orientation-imaging microscopy (OIM). It was found that cavity nucleation occurred along prior beta boundaries as well as at triple points; in particular, most cavities nucleated along boundaries perpendicular to the axial direction of the specimen. Extensive growth was observed for cavities surrounded by both hard and soft orientations, with the soft colonies accommodating more of the imposed strain. At high degrees of deformation, dynamic globularization of the colony microstructure adjacent to the cavities was also observed. In addition, the metallographic observations revealed that the cavities did not grow in an equiaxed mode, but in an elliptical manner. A tensor describing the cavity-growth rate along the axial, radial, and hoop specimen directions was determined using measurements of individual cavity sizes. The cavity-growth behavior in torsion was compared to previous observations from hot-tension tests. This comparison indicated that the rate of cavity growth in shear was approximately one-tenth that in uniaxial tension. This finding is in broad agreement with models predicting the variation of the cavity-growth rate as a function of the ratio of the mean stress to the hydrostatic stress.

I. INTRODUCTION

THE development of successful manufacturing techniques for metallic materials requires reliable information regarding hot-working characteristics. The proper hot-working temperature and deformation rate must be established in order to produce high-quality wrought products of complicated geometry. The control of internal cavitation is very important, because it helps avoid surface defects that reduce product yield and that may lead to poor service properties and premature failure.[1,2,3]

A considerable amount of research has been devoted to developing and understanding cavitation behavior for a wide range of metals and alloys.[4,5,6] For example, extensive work has been conducted to establish both the effect of the stress state on cavity growth and the determination of the conditions under which cavitation can be fully suppressed, or at least minimized. Also, previous experimental and analytical studies have focused on cavity-growth kinetics as a function of a stress parameter such as the ratio of the mean to effective stress. Most of these efforts dealt with stress ratios equal to or greater than the one imposed during tension testing, *i.e.*, 1/3, by employing techniques such as notched-tension testing,[7,8] equibiaxial-tension testing, and plane-strain tension.[9] There have also been investigations in which stress ratios below 1/3 were imposed, by the superposition of a hydrostatic compressive stress, on specimens deformed in tension.[10] By contrast, cavitation behavior under shear conditions has been evaluated, but to a lesser extent. A notable exception was the work of Bae *et al*.,[9] who conducted planar simple-shear tests for a modified 5083 aluminum alloy; they found that the extent of cavitation was finite, but was lower than that which occurred during uniaxial tension.

P.D. NICOLAOU is with S&B S.A., 106 72, Athens, Greece. Contact e-mail: p.nicolaou@sandb.com J.D. MILLER, Research Scientist, and S.L. SEMIATIN, Senior Scientist, are with the Air Force Research Laboratory, Materials and Manufacturing Directorate, AFRL/MLLM, Wright-Patterson Air Force Base, OH 45433-7817.

Manuscript submitted February 9, 2005.

The objective of the present work was to establish the effect of shear deformation on the cavitation behavior of the alpha/beta titanium alloy Ti-6Al-4V, with a colony-alpha microstructure, over a wider range of strains than that employed in the earlier work by Bae *et al*. for 5083 aluminum.[9] This material was chosen because of its widespread use in the aerospace industry and its known susceptibility to cavitation during primary hot working. To determine cavitation kinetics during simple-shear conditions, the hot-torsion test was used. Deformed specimens were characterized by optical, scanning-electron, and orientation-imaging microscopy (OIM). Cavity nucleation and growth characteristics were delineated with regard to the local colony orientations and imposed strains, and were compared to previous findings for the uniaxial- and notched-tension testing of Ti-6Al-4V with an identical (colony-alpha) microstructure.[7]

II. MATERIALS AND PROCEDURES

A. *Material*

The material used in the present work consisted of a 17.5-mm-diameter hot-rolled bar of Ti-6Al-4V with a fine, equiaxed-alpha microstructure in the as-received condition. The measured composition (in weight percent) was 6.25 aluminum, 4.05 vanadium, 0.19 iron, 0.19 oxygen, 0.012 carbon, 0.0004 hydrogen, 0.010 nitrogen, and balance titanium. The beta-transus temperature (the temperature at which $\alpha + \beta \rightarrow \beta$) for this alloy was 1000 °C. The material was heat treated at 955 °C/30 min + 1040 °C/3 min + 815 °C/10 min, and then air cooled. This treatment produced a mixed-colony, basketweave microstructure with a prior-beta grain size (and comparable colony size) of ~100 μm, and a grain-boundary alpha layer approximately 3-μm thick.

As shown by the alpha-phase (0002) pole figure of the heat-treated material (Figure 1), the texture of the Ti-6Al-4V alloy with the colony microstructure was relatively weak. The principal texture components comprised one with the *c*-axis parallel to the bar axis having an intensity of ~2.2 times random, and another characterized by the *c*-axis tilted ~60 deg

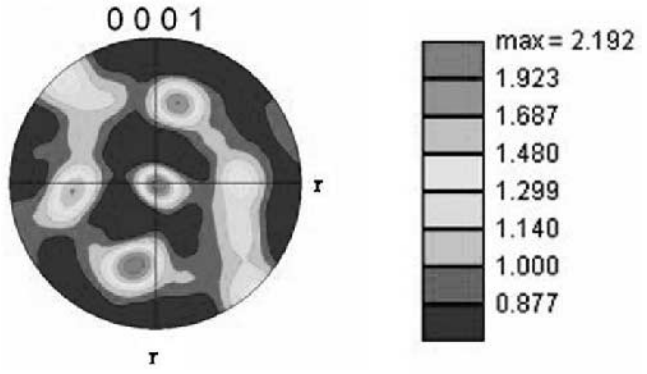

Fig. 1—The (0002) pole figure for the alpha phase of the Ti-Al-4V program material, following beta annealing.

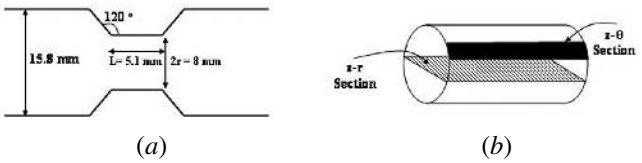

(*a*) (*b*)

Fig. 2—Schematic illustrations of (*a*) the torsion-specimen geometry and (*b*) the cross sections used in the metallographic analysis in the present work.

from the bar axis, with approximately 1.5 times random intensity. The slight asymmetry of the latter texture component suggested that the bar may have been fabricated using a Turks head mill, rather than a conventional bar mill.

B. *Torsion Testing*

Following heat treatment, solid round-bar torsion specimens having the geometry shown in Figure 2(a) were machined. The gage length of the specimen was equal to 5.1 mm, and its radius was equal to 4.0 mm. The total length of the specimen was equal to 150 mm. One end of each specimen was threaded, and the other had a notch, to fit the mating grips of the torsion apparatus. Such end designs were chosen to enable unconstrained cool-down of the specimen during water quenching following torsion, thus avoiding the introduction of additional damage following testing.

The torsion-testing apparatus was a custom-designed system that was built at the Air Force Research Laboratory. Being servohydraulic in nature, the system enables both the imposition of arbitrary loading/twisting schedules with or without intermediate dwell periods, and automated quenching at the completion of each test. Samples are heated using an indirect-resistance furnace with silicon-carbide heating elements. In the present work, fixed-end torsion tests were conducted at a temperature of 815 °C. This temperature was selected based on previous work at the same temperature, in which cavitation behavior under both uniaxial- and notched-tension conditions had been determined.[7] Following preheating and soaking at the test temperature for 10 minutes, torsion was conducted, using a constant twist rate of 4.8 deg/s, which corresponds to a surface von Mises effective strain rate of 0.04 s^{-1}. The test specimens were deformed to various final-twist angles between 90 and 250 deg, in order to impose different amounts of strain and, thus, to quantify the evolution of cavitation. The uniformity of strain along the gage length (and, hence, the absence of strain localization) developed using the specified deformation, and deformation-rate conditions were confirmed using fine, axial scribe lines that were machined on the surface of selected specimens.

C. *Optical Metallography and Image Analysis*

After torsion testing, each specimen was sectioned and prepared metallographically, to establish cavitation behavior. Two types of sections were utilized: an axial-diametral cross section containing the *z*-*r* plane and an axial-tangential section near the outer surface containing the *z*-θ plane (Figure 2(b)). On the *z*-*r* plane, cavities existed only at the outer edge of the specimen, where the strain was highest. The cavities analyzed were located in the region of highest strain. No transverse cross sections containing the *r*-θ plane were examined in this work. The cavity size and shape were measured using as-polished specimens, to avoid distortion of the damage features by acid etching. The important cavitation parameters were determined from optical micrographs shot at a magnification of 200 times, using the image-analysis software ImageJ Version 1.32 (National Institute of Health, USA). For each test, the number of cavities examined ranged between 40 and 80. Because the cavities were not equiaxed, they were approximated in the image analysis as being elliptical in shape. The cavitation parameters so obtained included the cavity area, the length of the major and minor axes of each cavity, and the angle between the major axis of the ellipse (cavity) and the axial (*z*) direction of the specimen. The deviation of the ellipses used to approximate the cavities to the actual cavity shape was assessed by comparing the actual cavity area to that calculated from the ellipse axes. It was found that the maximum deviation for the great majority of the cavities was below 5 pct, while only very few cavities had deviations of up to 10 pct.

D. *Scanning Electron Microscopy*

Specimen sections were also examined *via* backscattered electron (BSE) imaging and electron backscattered diffraction (EBSD) pattern analysis in a scanning electron microscope (SEM), to establish the microstructure and colony orientation in the vicinity of a number of cavities. For this purpose, samples were electropolished in a solution of 590-mL methanol, 350-mL 2-butoxy ethanol, 60-mL $HClO_4$ (60 pct) at 20 VDC with a stainless steel cathode with moderate agitation for ~1 hour, to remove approximately 5 μm of material. Subsequent BSE and EBSD examinations were conducted with a Leica 360FE SEM (Leica Microsystems Inc.). Analysis by OIM, based on the EBSD patterns, was facilitated using TEXSEM†

†TEXSEM is a trademark of TEXSEM Laboratories Inc.

Laboratories (TSL) software (Version 2.6); details of the OIM analysis for Ti-6Al-4V with a colony microstructure are summarized elsewhere.[11,12] In brief, scans that consisted of ~15,000 data points were conducted around a number of cavities. Data sets in which either indexing was not possible or the confidence in correct indexing was low, were "cleaned", employing a nearest-neighbor criterion in order to replace the orientation of pixels to the orientation of the neighbor with the highest confidence index value.

III. THEORETICAL BACKGROUND

Prior to presenting and discussing the results from this project, the fundamental relations used to describe torsion testing and cavity-growth phenomena are summarized here.

A. *Hot-Torsion Testing*

Torsion testing under fixed-end conditions consists of a simple-shear mode of deformation. The extent of deformation and the deformation rate depend on the twist angle and specimen geometry. In particular, the following relationships hold during torsion:[13]

$$\gamma = \frac{r\theta}{L} \text{ and } \dot{\gamma} = \frac{r\dot{\theta}}{L} \quad [1]$$

in which γ is the engineering shear strain (equal to twice the tensorial shear strain), θ is the twist angle (in radians), r is the radial position, L is the gage length, $\dot{\gamma}$ is the shear strain rate, and $\dot{\theta}$ is the twist rate (in radians per unit time). For a given twist angle θ, large values of r and small values of L promote high values of γ. Similarly, large r and small L values result in large values of $\dot{\gamma}$ for a given $\dot{\theta}$. Values for γ and $\dot{\gamma}$ vary with the radius in a solid bar or thick-wall tube; they are greatest at the surface and vanish at the center. As is the typical convention, the values of strain and strain rate reported in this work are those that pertain to the surface of the specimen. When torsion data are compared to measurements obtained from other deformation modes, it is this strain and this strain rate that are usually important.

The shear strain and shear-strain rate can be converted to the von Mises effective strain and strain rate (denoted as $\bar{\varepsilon}$ and $\dot{\bar{\varepsilon}}$, respectively), according to the following relationships:

$$\bar{\varepsilon} = \frac{\gamma}{\sqrt{3}} \text{ and } \dot{\bar{\varepsilon}} = \frac{\dot{\gamma}}{\sqrt{3}} \quad [2]$$

Likewise, torque data can be converted to effective stress, according to the following relationship:

$$\bar{\sigma} = \frac{(3 + n + m)\sqrt{3}}{2\pi R^3} M \quad [3]$$

in which M denotes the torque, $\bar{\sigma}$ is the effective stress, R denotes the sample outer radius, and n and m are approximately equal to the strain-hardening and strain-rate sensitivity exponents, respectively.

B. *Cavitation*

For plasticity-controlled growth under uniaxial-tension conditions, it has been shown that the cavity-volume fraction, C_V, usually has an exponential dependence on strain,[4,14,15] *i.e.*,

$$C_V = C_{V0} \exp(\eta_{APP} \varepsilon) \quad [4]$$

Similarly, for equiaxed cavities, the cavity-area fraction, C_A, equals the cavity-volume fraction, and is described by

$$C_A = C_{A0} \exp[(\eta_{APP}/2)\varepsilon] \quad [5]$$

In Eqs. [5] and [6], C_{V0} and C_{A0} denote the initial volume and area fraction, respectively, ε denotes the axial strain (=the effective strain in tension), and η_{APP} is the apparent cavity-growth rate that takes into account the influence of both continuous nucleation and coalescence.

For the growth of an individual, equiaxed (spherical) cavity of initial volume V_0 (and radius r_0), the following relationships apply:

$$V = V_0 \exp(\eta\varepsilon) \text{ and } r = r_0 \exp[(\eta/3)\varepsilon] \quad [6]$$

in which η is the individual cavity-growth parameter, and V and r equal the instantaneous cavity volume and radius, respectively. For cavities with an ellipsoidal (rather than spherical) shape, the change of the size of a cavity in a particular direction may be described by the following relation:

$$L_i = L_{i0} \cdot \exp(\eta_i \varepsilon) \quad [7]$$

in which L denotes size, the subscript i denotes the direction, and η_i is the cavity-growth-rate parameter for the direction i.

Cavity growth is also influenced by the imposed stress state. Nevertheless, relations identical to those described here may be applied for nonuniaxial states of stress, provided the stress-state-dependent value of η is used and ε is replaced by the effective strain $\bar{\varepsilon}$.

IV. RESULTS AND DISCUSSION

The results of this work are presented and discussed in three broad subsections. The first deals with the stress-strain behavior. The second summarizes the microscopic analysis of cavity nucleation and growth and the influence of local texture (as determined from OIM) on cavitation. The third subsection deals with the determination of the meso-macroscale cavitation parameters, such as the cavity-nucleation rate and the directionality of the cavity-growth rate.

A. *Stress-Strain Behavior*

The effective stress-effective strain curve for the specimen that was twisted 250 deg, determined from Eqs. [1] through [3], is presented in Figure 3. The flow behavior of Ti-6Al4V

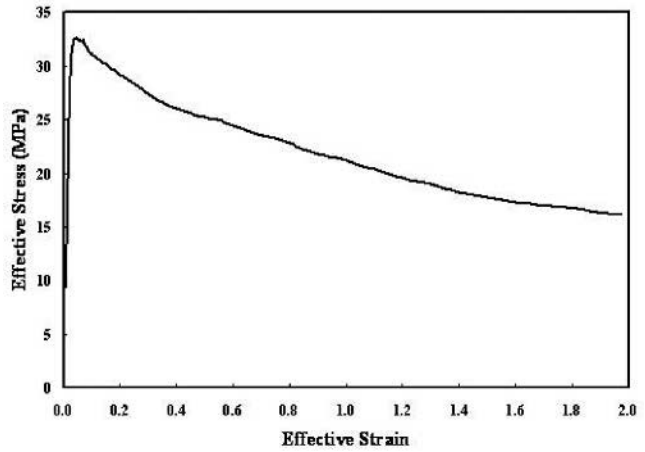

Fig. 3—Effective stress-strain curve for Ti-6Al-4V deformed at 815 °C and at a surface effective strain rate of 0.04 s^{-1}.

with the transformed (colony/Widmanstätten) microstructure exhibited marked flow softening at hot-working temperatures. This softening occurred continuously throughout the entire deformation. The fitting of the stress-strain data with a power-law relationship ($\bar{\sigma} \cong \bar{\varepsilon}^{n}$) indicated that the flow-softening exponent n was equal to -0.23. This value of n is very close to that determined previously for a similar material tested in compression, *i.e.*, $n = -0.22$.[16]

B. *Cavitation Observations and Mechanism*

1. *Cavitation observations from optical metallography*

The examination of optical micrographs revealed that cavities nucleated (and subsequently grew) at the prior-beta grain boundaries, as well as at triple points (Figure 4). It was also observed that the largest number of cavities was located along the prior-beta grain boundaries, which were perpendicular or nearly perpendicular (*i.e.*, within 15 deg) to the axial direction of the specimen. However, a small number of cavities were also found to have nucleated along boundaries that were parallel to the torsion-specimen axis.

The location of the nucleation site affected the subsequent growth and the shape of each cavity, for a given imposed deformation. For example, as shown in Figure 4, the most rapid cavity growth occurred primarily parallel to the prior-beta grain boundaries (*e.g.*, the location marked A), thus resulting in cavities with cross sections that were elliptical in shape. In addition, a comparison of micrographs on the z-θ and z-r planes suggested that most of the grain-boundary cavities were actually ellipsoidal, with the shortest (minor) axis parallel to the z direction. In contrast to the characteristics of cavities lying on the prior-beta grain boundaries, cavities that had nucleated at grain-boundary or colony-triple points appeared to have grown in a more isotropic fashion, leading to a roughly equiaxed shape (*e.g.*, location B in Figure 4).

2. *The OIM analysis*

The fact that the cavities did not lie at 45 deg to the torsion axis may seem surprising, inasmuch as the principal directions of stress and strain lie along such directions. However, this finding can be rationalized in view of the fact that the Ti-6Al-4V program material was not an isotropic continuum. Rather, this material was composed of colonies of alpha platelets with different orientations that would be expected to deform differently relative to the externally applied loading. As a result, preferential sites for cavity nucleation as well as preferential directions of growth might be expected, as were observed. In this regard, therefore, additional insight into cavity nucleation and growth was gained from OIM results, for colonies surrounding various cavities. With this information, qualitative insight into the observed anisotropic cavitation behavior was obtained.

Inverse-pole-figure (IPF) maps, Taylor-factor maps, and BSE results from z-θ cross sections of two specimens, one twisted 90 deg (surface-effective strain ≈ 0.7) and the other 225 deg (surface-effective strain ≈ 1.78), revealed the impor-

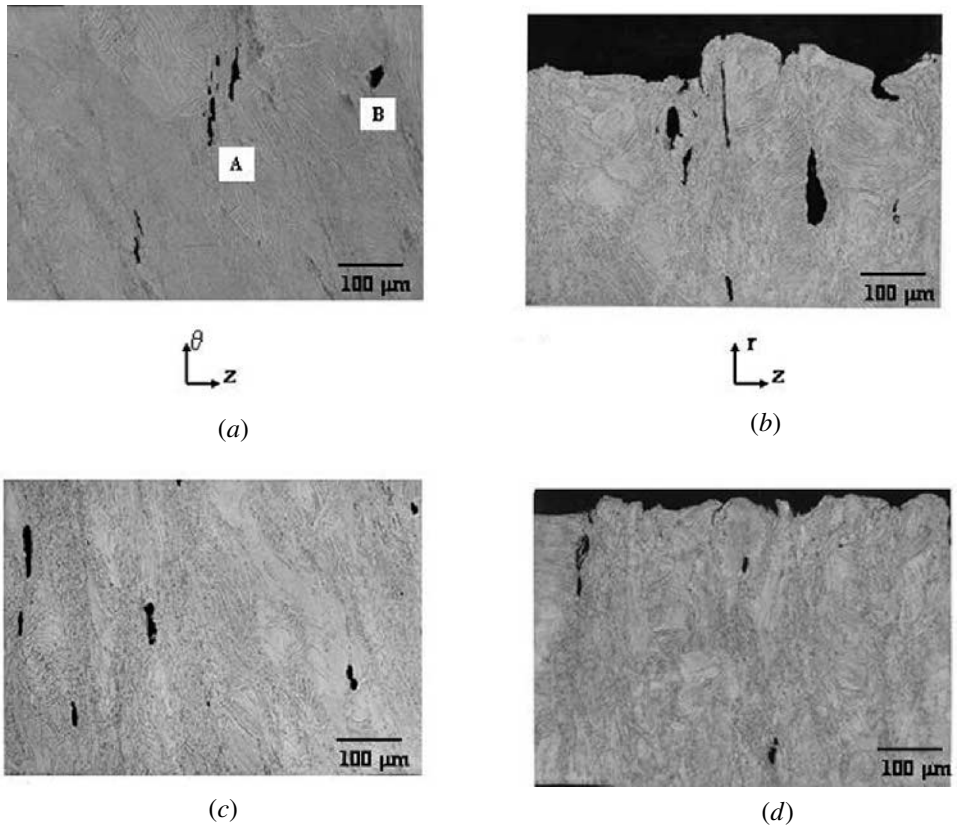

Fig. 4—Micrographs of the z-r and z-θ cross sections revealing the location and shape of cavities. The macroscopic effective strains were (*a*) 1.07, (*b*) 1.78, (*c*) 1.98, and (*d*) 1.78.

tant effects of the local colony orientation on cavity nucleation and growth (Figures 5 and 6).* In all cases, alpha-phase IPF (orientation) maps for the tensile-strain direction in torsion (45 deg, with respect to the axial direction of the specimen) are shown. The orientations of a number of colonies are also indicated, with overlaid hexagonal unit-cell prisms. The colors in Figures 5 and 6 are based upon the standard red-green-blue convention, such that the red colonies have their *c*-axes aligned along the tensile strain direction. In addition to the IPF maps, Taylor-factor maps for the alpha-phase deformation were computed in the same way as described in Reference 17. In brief, the TSL software was employed to compute such maps, assuming simple-shear deformation and a critical resolved shear stress (CRSS) ratio of 0.7:1:3 for prism <a>, basal <a>, and pyramidal <c + a> slip. The Taylor-factor maps are shown using a gray scale, with the lightest shades corresponding to the hardest orientations in simple shear, and the darkest shades to the softest ones.

In the specimen twisted only 90 deg (Figures 5(a) and (b)), the cavities were relatively small, and thus were likely to have grown only a small amount following nucleation. In Figure 5(a), two cavities were nucleated at a prior-beta

*In several cases, the BSE and OIM cavity images did not appear to coincide exactly. Such differences were determined to be an artifact associated with the distortion arising from the 70-deg specimen tilt during EBSD.

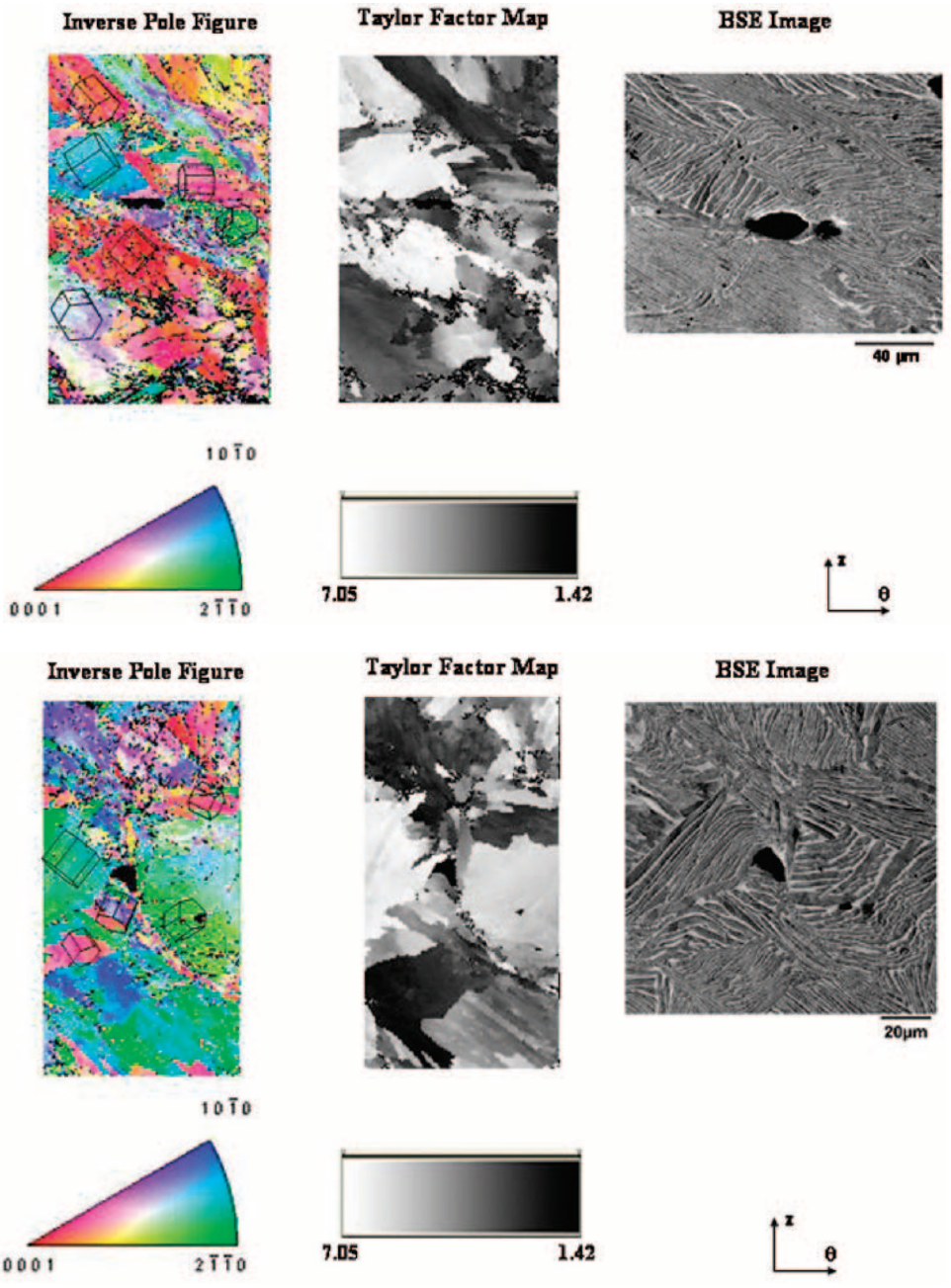

Fig. 5—The IPF maps for the tensile-strain direction, Taylor-factor maps for simple-shear deformation, and BSE micrographs of z-θ cross sections of a specimen twisted 90 deg.

grain boundary nearly perpendicular to the axial direction of the specimen. The cavities are surrounded primarily by colonies of soft orientations, while hard orientations are also present, which would have produced substantial strain incompatibility. It appears that the two cavities grew mainly along the prior-grain boundary and began to coalesce to form an elliptical cavity.

The sample twisted 90 deg also revealed a more-or-less equiaxed cavity (Figure 5(b)); this cavity appeared to have nucleated at a triple point. In this case, the cavity was surrounded by several colonies with soft orientations, but there were some hard orientations as well. This example is similar to those found previously for the uniaxial-tension deformation of Ti-6Al-4V with a colony-alpha microstructure.[17] The location of the cavity and the geometry and strength of the surrounding colonies permitted the cavity to grow in an equiaxed manner. A second, smaller cavity with a diameter of about 4.5 μm was also found nearby (Figure 5(b)). This cavity appears to have nucleated at an alpha-platelet/ beta-matrix interface perpendicular to the z-direction of the specimen that lies within a colony, not at a colony or grain boundary.

The cavities formed in the sample twisted to 225 deg (Figures 6(a), (b), and (c)) were substantially larger than those in the 90-deg sample. For example, Figure 6(a) shows a very large cavity (major axis $\approx$ 500 μm), which nucleated at a boundary that was perpendicular to the z-axis. Above and to the left of the cavity, there was a colony with a hard orientation. Although the alpha platelets in this colony were bent,

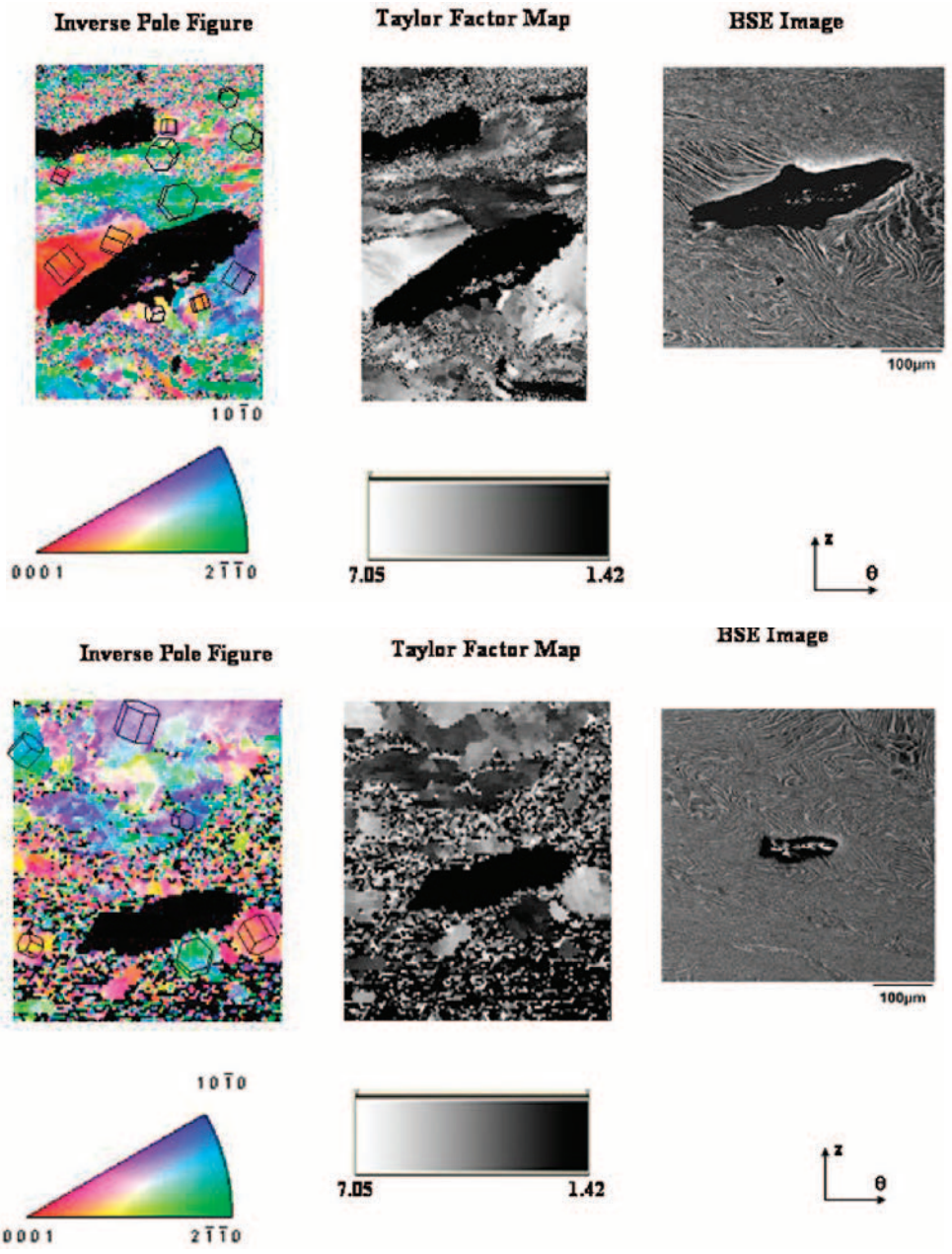

Fig. 6—The IPF maps for the tensile-strain direction, Taylor-factor maps for simple-shear deformation, and BSE micrographs of z-θ cross sections of a specimen twisted 225 deg.

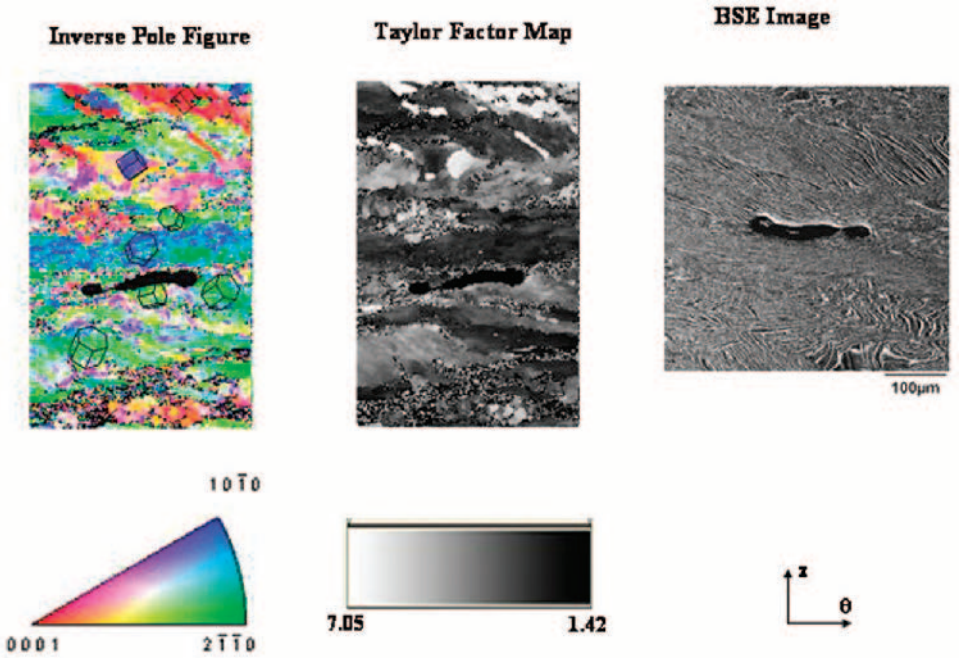

Fig. 6—(Continued). The IPF maps for the tensile-strain direction, Taylor-factor maps for simple-shear deformation, and BSE micrographs of z-θ cross sections of a specimen twisted 225 deg.

they had undergone only a very limited amount of globularization. This observation is analogous to the previous results from compression tests on Ti-6Al-4V with a comparable colony microstructure and platelet thickness.[11,18] The micrographs also suggest that the cavity grew primarily by the deformation of the softer colonies directly below it. As shown in both the BSE and OIM images, the high strains here led to the breakup and globularization of the colony-alpha microstructure.

Another large cavity is shown in Figure 6(b). There was a hard-colony microstructure below and to the right of it, but a significant amount of globularization had developed elsewhere, as can be seen in the OIM and BSE images. It can thus be concluded that cavity growth was encouraged by the presence of soft colonies that accommodated a large amount of strain during cavity growth.

A final example in the sample twisted 225 deg is shown in Figure 6(c). Most probably, the cavity in this case had grown along a prior-beta grain boundary or a colony boundary, inasmuch as the location is not fully elucidated by the BSE image. This cavity did not appear to border any colonies with hard orientations, but was surrounded by soft orientations only. This cavity grew mostly in a cracklike fashion along the grain boundary, somewhat unlike the cavities in Figures 6(a) and (b). It also appears that the final cavity was formed by the coalescence of two discrete cavities. Furthermore, the overall degree of globularization was smaller in this instance, because the deformation was more uniformly distributed, thus avoiding the generation of the required large local strains.

Overall, the OIM results and corresponding BSE images provided substantial insight into the interaction of cavitation and the nonuniformity of the local plastic flow, as surmised from the globularization observations. First, the observations revealed that when both hard and soft orientations were present, cavities grew more extensively. This is most likely a result of the fact that the externally applied strain was accommodated primarily by the soft colony.[19] Because cavities grew *via* the deformation of the soft orientation,[17] the cavity-growth strain was much higher than the macroscopic one. Therefore, per Eq. [6], the final cavity size may be expected to be larger than that based on the macroscopic (imposed) strain alone. The same rationale explains the dynamic globularization that took place in some of the colonies that bordered the cavities. For the 225-deg torsion test, for example, the macroscopic effective strain was 1.78. However, this strain was not equally partitioned among the various colonies. The soft ones accommodated much higher levels of deformation and, as a result, underwent dynamic globularization, while the hard ones, which deformed very little, maintained their initial structure to a great extent. These observations can be compared to earlier work involving uniaxial compression at the same deformation temperature and a comparable strain rate,[18] and torsion at the same temperature (but at a lower strain rate, of the order of 10^{-3} s^{-1}).[20] The macroscopic effective strains required to initiate and complete dynamic globularization were of the order of 1 and 2.5, respectively, for uniaxial compression, and 0.4 and 1.4, respectively, for torsion. However, these strains would be expected to be nonuniformly accommodated by hard *vs* soft colonies. It may be hypothesized, therefore, that the local strain required to initiate globularization (in soft colonies) is somewhat greater than ~0.5 to 1, while that required to complete globularization (in hard colonies) is somewhat less than ~2.

3. *Interpretation of cavitation mechanism*

As deduced from the optical/BSE micrographs and OIM results, the majority of cavity nucleation occurred at the prior-beta grain boundaries. The role of grain-boundary alpha, as suggested in previous work,[21] appears to have its greatest effect on cavity nucleation through the development of constraints that affect the growth from the nanometer to

micrometer scale. Once cavities reach the micrometer size, cavity growth is less highly constrained and, hence, more likely controlled by a general, albeit anisotropic, plasticity model, such as that suggested by the present observations. Furthermore, most of such grain-boundary nucleation sites were perpendicular to the axial direction (torsion axis) of the specimen. It was also observed that the cavity growth led to an elliptical shape. From these observations, a cavitation mechanism may be hypothesized. In particular, a plausible explanation is that cavity nucleation was controlled by shear failure at the prior-beta grain boundaries. Such failure may occur by either grain-boundary sliding or shear localization in the thin layer of the beta phase between the grain-boundary alpha and the colony alpha. Such a mechanism, *i.e.*, shear failure of the beta grain boundaries, is plausible in view of the fact that it explains the following: (1) the nucleation of penny-shaped initial flaws along the grain-boundary. These flaws then grow transverse to the grain boundary under the action of the tensile component of stress induced during simple-shear deformation; (2) the preferential nucleation on boundaries perpendicular to the torsion axis, because the imposed shear stress is largest for such boundaries; and (3) the fact that nucleation at the boundaries between colonies is limited, because such boundaries are not straight and, thus, intercolony sliding is impeded.

C. *Cavitation Parameters*

1. *Evolution of cavity shape and orientation with strain*

The evolution of the cavity shape was quantified as a function of the equivalent cavity radius, defined as $\sqrt{A/\pi}$, in which A denotes the cavity area. Figure 7 shows the average cavity-aspect ratio as a function of the equivalent cavity radius, for cavities observed in the z-θ cross section. The aspect ratio increases with both increasing cavity size and strain. This finding is consistent with the observations in Section IV, which revealed that cavities grew faster in the θ (and r) directions compared to the z direction.

2. *Cavity-nucleation rate*

Metallographic observations revealed that cavities nucleated continuously as deformation proceeded. The cavity-nucleation rate was determined from the slope of a plot of the cavity-population density as a function of effective strain, for cavities observed in both z-r and z-θ sections (Figure 8). For the range of strains used in the current work, the results indicated that the cavity nucleation was essentially identical, irrespective of the plane of observation. However, it can be deduced that, for strains between 0.7 and 2.0, the rate itself was relatively small, *i.e.*, ~15 cavities/mm^2/unit strain. This value is comparable to that observed previously (~10 to 50 cavities/mm^2/unit strain) during the hot-tension testing of Ti-6Al-4V with a colony-alpha microstructure.[15]

It may seem surprising that the cavity-population density increased with strain, despite the fact that the material exhibited flow softening, at least based on macroscopic stress-strain measurements, *i.e.*, cavity nucleation continued under decreasing stress conditions. This behavior can be rationalized on the basis of the distortion of the prior-beta grains (and colonies) during torsion (*e.g.*, BSE images of Figures 5 and 6). This distortion changes grains/colonies that were originally equiaxed into elliptical grains/colonies. Segments of the boundaries of these elliptical grains rotate toward the transverse direction of the specimen and, in so doing, the shear stress resolved along these segments increases. Therefore, cavity nucleation is controlled by two competing mechanisms: the reduction of the macroscopic stress and the increase of the shear stress resolved along the prior beta boundaries due to the distortion and rotation of the prior-beta grains.

3. *Cavity-growth rate*

Cavity growth was quantified in terms of both (1) the apparent (average) growth rate in the z-r and z-θ planes (determined from the change of the cavity-area fraction as a function of strain) and (2) the directional cavity-growth rate along the z, r, and θ specimen axes.

The apparent (average) cavity-growth rate (η_{APP}) was determined for observations on both the z-r and the z-θ sectioning planes *via* semilog plots of the average cavity-area fraction, as a function of the effective strain (Figure 9). The cavity fraction was higher in the z-θ plane than the z-r plane, indicating that cavities did not grow isotropically. However, the values of $\eta_{APP_{z\text{-}r}}$ and the $\eta_{APP_{z\text{-}\theta}}$ were found to be comparable, *i.e.*, 0.71 and 0.75, respectively. This

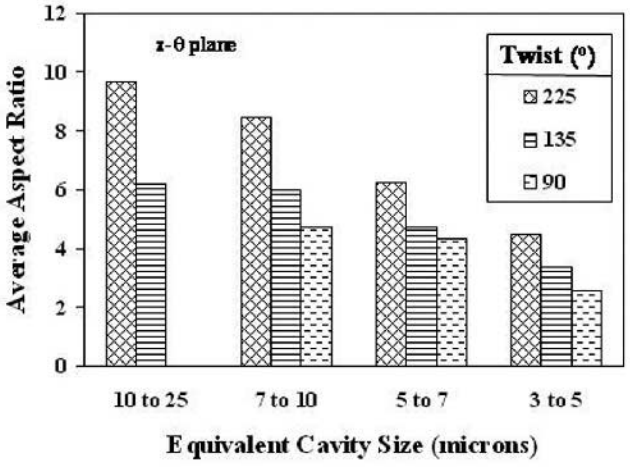

Fig. 7—Evolution of the average cavity-aspect ratio and size as a function of twist angle.

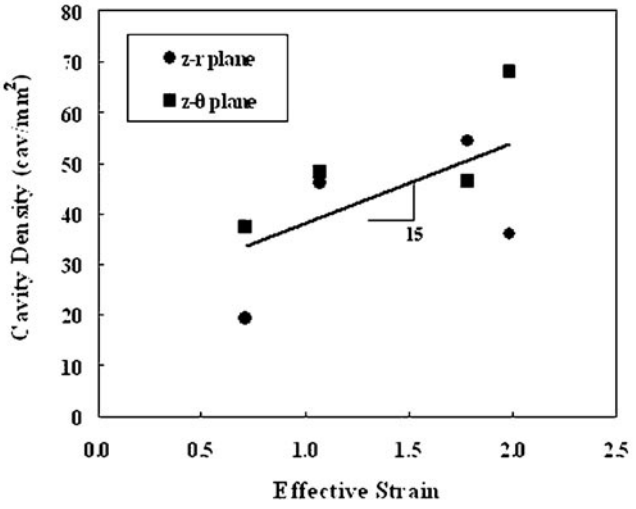

Fig. 8—Cavity-population density as a function of effective strain for the z-r and z-θ cross sections.

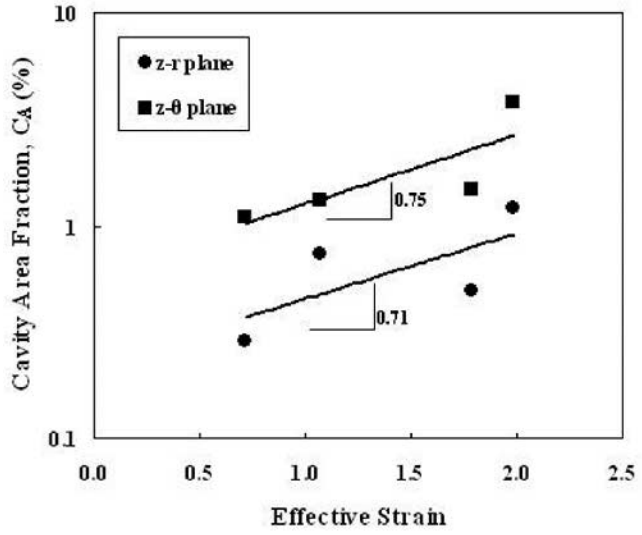

Fig. 9—Variation of the cavity area with strain, for the z-r and $z-\theta$ cross sections.

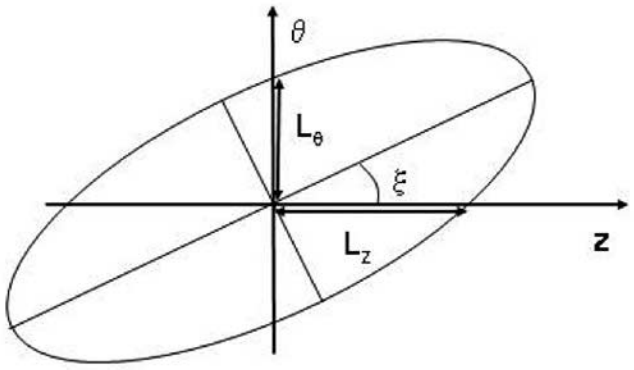

Fig. 10—Definition of the geometric parameters used to describe the cavity geometry.

finding implies that the overall growth in the z-r and z-θ planes was essentially equal, despite the fact that cavity growth was anisotropic, as seen from the elliptical cavity shapes.

Directional cavity-growth rates were determined in order to quantify the development of ellipsoidal cavities during torsional deformation. Specifically, the cavity-growth rate along the three specimen directions (z, r, θ) was determined using cavity-size measurements on the z-r and z-θ cross sections. When the principal axes of the ellipse/ellipsoid were parallel to the z, r, θ directions, the pertinent cavity lengths were determined directly. As discussed in Section IV, however, some of the cavities had axes that were not aligned exactly with the z, r, and θ directions. Therefore, the cavity size along each of the specimen directions was calculated as shown in Figure 10. Specifically, the lengths L_θ and L_z were determined from the cavity geometry (*i.e.*, major- and minor-axis lengths), and from the angle between the major axis and the z-axis, using straightforward trigonometric calculations.

The average cavity lengths (L_z, L_r, and L_θ are plotted against the effective strain, in Figure 11. These results indicate that the directional cavity-growth rate was highest

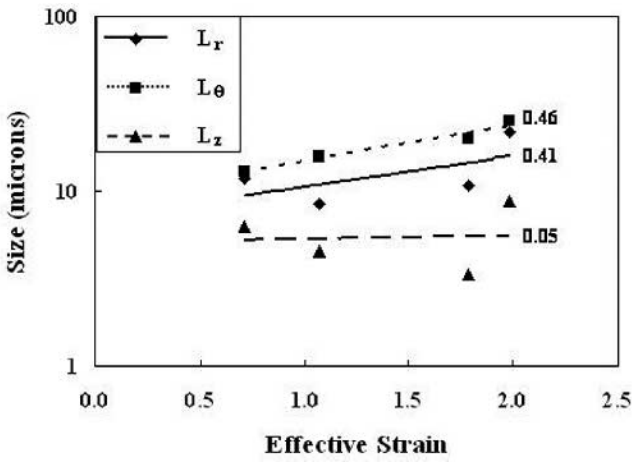

Fig. 11—Evolution of the cavity size along the three specimen directions (z, r, θ), as a function of effective strain.

in the θ direction, lower in the r-direction, and very small in the z-direction. From the results of Figure 11, it can be concluded that the cavity-growth parameter, usually reported as a scalar quantity, is actually a tensor $\{\eta\}$, *i.e.*,

$$\{\eta\} = \begin{pmatrix} \eta_z & & \\ & \eta_r & \\ & & \eta_\theta \end{pmatrix} = \begin{pmatrix} 0.05 & & \\ & 0.41 & \\ & & 0.46 \end{pmatrix}$$

The volumetric cavity-growth rate η equals the sum (trace) of the components of the above tensor, *i.e.*,

$$\eta = \eta_z + \eta_r + \eta_\theta \text{ or } \eta = 0.92$$

A comparison of η_{APP} and η reveals that the ratio η_{APP}/η is less than the unity, a finding that contrasts with previous analytical modeling work.[22] This apparent contradiction can be explained by the fact that the cavities in the present work were ellipsoidal and not equiaxed, as assumed in the modeling work of Reference 22. Therefore, the cavity-area fraction determined from one or more planes cannot be assumed to be equal to the cavity-volume fraction. On the other hand, if η_{APP}/η is estimated for a particular plane, then it is, indeed, higher than unity. For example, for the z-θ plane, $\eta_{APP} = 0.75$ and $\eta_z + \eta_\theta = 0.51$; $\eta_{APP}/\eta = 1.47$, *i.e.*, greater than unity. Similarly, η_{APP}/η for the z-r plane is found to be equal to 1.54.

4. *Comparison of the cavity-growth rate in shear to model predictions*

The cavity-growth rate determined from the present work in simple shear was compared both to the previous measurements on Ti-6Al-4V (with a nearly identical microstructure) tested in other stress states and to the predictions of several models. Previous work at the same temperature and strain rate,[23] for example, indicated that the cavity-growth rate under uniaxial-tension conditions was equal to ~9. Therefore, the ratio of the cavity-growth rate in simple shear *vs* that in tension is $\eta_{shear}:\eta_{tension} = 0.1$.

As described in numerous previous theoretical and experimental investigations,[7,10,15,23] the effect of an arbitrary deformation state on cavity growth is usually interpreted in terms

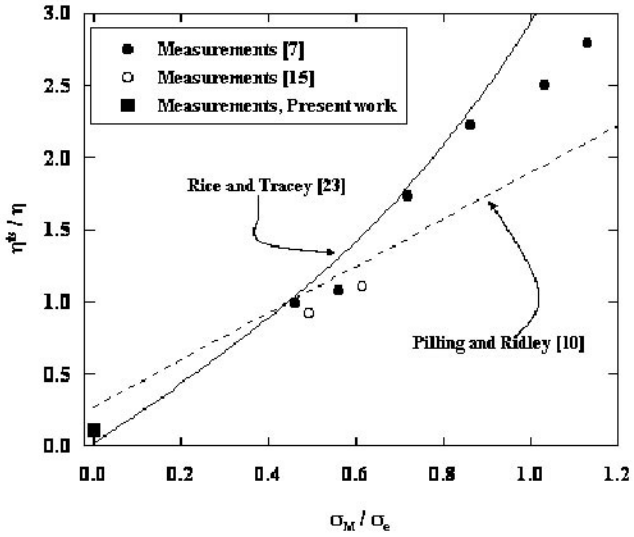

Fig. 12—Comparison of model predictions and experimental measurements of the normalized cavity-growth rate, as a function of the stress ratio σ_M/σ_e for Ti-6Al-4V with a colony-alpha microstructure.

of the dependence of the cavity-growth parameter for the specific stress state (η^{ts}) on the ratio of the mean to effective stress, *i.e.*, σ_M/σ_e, as shown in Figure 12. In this figure, the cavity-growth parameter (η^{ts}) (plotted on the ordinate) has been normalized by the rate in tension (denoted simply as η). The continuous lines are predictions from the Pilling-and-Ridley (P + R)[10] and Rice-and-Tracey (R + T)[24] models. The round data points correspond to earlier measurements for tension and notched-tension tests on Ti-6Al-4V with an almost identical microstructure.[7,15] For simple shear, $\sigma_M = 0$, and thus $\sigma_M/\sigma_e = 0$. The square data point, corresponding to the present torsion results, has therefore been plotted at $\sigma_M/\sigma_e = 0$. This datum lies between the P + R and R + T models, but is closer to the R + T prediction.

V. SUMMARY AND CONCLUSIONS

Cavity initiation and growth behavior in Ti-6Al-4V deformed under simple-shear conditions was established using hot-torsion testing. The experiments were conducted at 815 °C/0.04 s^{-1} and a range of twist angles between 90 and 250 degrees, corresponding to surface effective strains between 0.7 and 2.0. Optical and scanning-electron microscopy revealed that most cavities nucleated at boundaries perpendicular to the axial direction of the specimen; the location of cavity nucleation affected the subsequent cavity growth. Using OIM, it was found that the presence of adjacent hard- and soft-colony orientations appeared to promote the most rapid cavity growth. The nonuniform deformation associated with such hard and soft orientations was mirrored in observations of local dynamic globularization. The vast majority of cavities grew in an ellipsoidal, not an equiaxed, manner, as quantified by growth measurements along the axial, radial, and hoop directions of the torsion specimens. Hence, it was concluded that the cavity-growth rate should be formulated as a tensor, not a scalar, quantity. The measured ratio of the volumetric cavity-growth rate in shear to that in tension was in broad agreement with model predictions and previous trends derived from experiments in other, higher-triaxiality, stress states.

ACKNOWLEDGMENTS

This work was conducted as part of the in-house research activities of the Metals Processing Group of the Air Force Research Laboratory's Material and Manufacturing Directorate. The support and encouragement of the laboratory management and the Air Force Office of Scientific Research (Dr. C.S. Hartley, program manager) are gratefully acknowledged. Two of the authors were supported under Air Force Contract Nos. F33615-00-C-5212 (PDN) and F33615-03-D-5801 (JDM). The assistance of Messrs. P.N. Fagin and N.D. Frey in conducting the torsion tests is also much appreciated.

REFERENCES

1. C.C. Bampton and J.W. Edington: *J. Eng. Mater. Technol*., 1983, vol. 105, pp. 55-60.
2. M.B. Taylor, H.M. Zbib, and M.A. Khaleel: *Int. J. Plasticity*, 2002, vol. 18, pp. 415-42.
3. P.D. Nicolaou, R.E. Bailey, and S.L. Semiatin: in *Handbook of Workability and Process Design*, G.E. Dieter, H.A. Kuhn, and S.L. Semiatin, eds., ASM International, Materials Park, OH, 2003, pp. 68-85.
4. B.P. Kashyap and M.K. Mukherjee: *Res Mechanica*, 1986, vol. 17, pp. 293-355.
5. A.H. Chokshi: *J. Mater. Sci*., 1986, vol. 21, pp. 2073-80.
6. R. Verma, P.A. Friedman, A.K. Ghosh, S. Kim, and C. Kim: *Metall. Mater. Trans. A*, 1996, vol. 27A, pp. 1889-98.
7. P.D. Nicolaou, R.L. Goetz, and S.L. Semiatin: *Metall. Mater. Trans. A*, 2004, vol. 35A, pp. 655-63.
8. H. Agarwal, A.M. Gokhale, S. Graham, and M.F. Horstemeyer: *Mater. Sci. Eng. A*, 2003, vol. 341 (no. 1-2), pp. 35-42.
9. D.H. Bae, A.K. Ghosh, and J.R. Bradley: *Metall. Mater. Trans. A*, 2003, vol. 34A, pp. 2449-63.
10. J. Pilling and N. Ridley: *Acta Metall*., 1986, vol. 34, pp. 669-79.
11. T.R. Bieler and S.L. Semiatin: *Int. J. Plasticity*, 2002, vol. 18, pp. 1165-89.
12. T.R. Bieler and S.L. Semiatin: in *Lightweight Alloys for Aerospace Applications VI*, PDF Only Edition, K.V. Jata, ed., TMS, Warrendale, PA, 2001, pp. 161-70.
13. S.L. Semiatin and J.J. Jonas: in *Handbook of Workability and Process Design*, G.E. Dieter, H.A. Kuhn, and S.L. Sematin, eds., ASM International, Materials Park, OH, 2003, pp. 86-121.
14. J. Pilling and N. Ridley: in *Superplasticity in Aerospace*, H.C. Heikkenen and T.R. McNelley, TMS, Warrendale, PA, 1988, pp. 183-97.
15. P.D. Nicolaou and S.L. Semiatin: *Acta Mater*., 2003, vol. 51, pp. 613-23.
16. R.M. Miller, T.R. Bieler, and S.L. Semiatin: *Scripta Mater*., 1999, vol. 40, pp. 1387-93.
17. T.R. Bieler, P.D. Nicolaou, and S.L. Semiatin: *Metall. Mater. Trans. A*, 2005, vol. 36A, pp. 129-40.
18. S.L. Semiatin, V. Seetharaman, and I. Weiss: *Mater. Sci. Eng. A*, 1999. vol. A263, pp. 257-71.
19. S.L. Semiatin, F. Montheillet, G. Shen, and J.J. Jonas: *Metall. Mater. Trans. A*, 2002, vol. 33A, pp. 2719-27.
20. R.M. Roths, G. Angella, B.P. Wynne, W.M. Rainforth, S.L. Semiatin, and J.H. Beynon: *Metall. Mater. Trans. A*, 2004, vol. 35A, pp. 2993-3001.
21. A.K. Ghosh, D.H. Bae, and S.L. Semiatin: *Mater. Sci. Forum*, 1999, vols. 304–306, pp. 609-16.
22. P.D. Nicolaou, S.L. Semiatin, and A.K. Ghosh: *Metall. Mater. Trans. A*, 2000, vol. 31A, pp. 1425-34.
23. S.L. Semiatin, V. Seetharaman, A.K. Ghosh, E.B. Shell, M.P. Simon, and P.N. Fagin: *Mater. Sci. Eng. A*, 1998, vol. A256, pp. 92-110.
24. J.R. Rice and D.M. Tracey: *J. Mech. Phys. Solids*, 1969, vol. 17, pp. 201-17.